Study of Excited Ξ Baryons in $\bar{p}p$-Collisions with $\overline{\text{P}}$ANDA

Authors:

Jennifer Pütz, Albrecht Gillitzer, James Ritman

Abstract

Understanding the excitation pattern of baryons is indispensable for a deep insight into the mechanism of non-perturbative QCD. Up to now only the nucleon excitation spectrum has been subject to systematic experimental studies while very little is known on excited states of double or triple strange baryons.
In studies of antiproton-proton collisions the $\overline{\mathrm{P}}$ANDA experiment is well-suited for a comprehensive baryon spectroscopy program in the multi-strange and charm sector. A large fraction of the inelastic $\bar{\mathrm{p}}\mathrm{p}$ cross section is associated to final states with a baryon-antibaryon pair together with additional mesons, giving access to excited states both in the baryon and the antibaryon sector.
In the present study we focus on excited Ξ states. For final states containing a $\Xi\ \bar{\Xi}$ pair cross sections up to the order of μb are expected, corresponding to production rates of $\sim 10^6$/d at a Luminosity $L = 10^{31}\,\mathrm{cm}^{-2}\,\mathrm{s}^{-1}$ (5% of the full value). A strategy to study the excitation spectrum of Ξ baryons in antiproton-proton collisions will be discussed. The reconstruction of reactions of the type $\bar{\mathrm{p}}\mathrm{p} \rightarrow \Xi\ {*}\ \bar{\Xi}$ (and their charge conjugated) with the $\overline{\mathrm{P}}$ANDA detector will be presented based on a specific exemplary reaction and decay channel.

Contents

1 Event generation

To study excited Ξ baryons the simulation of signal events is needed. For this study 1.5 million signal events have been generated. The decay channel for the simulation is shown in figure 1.1.

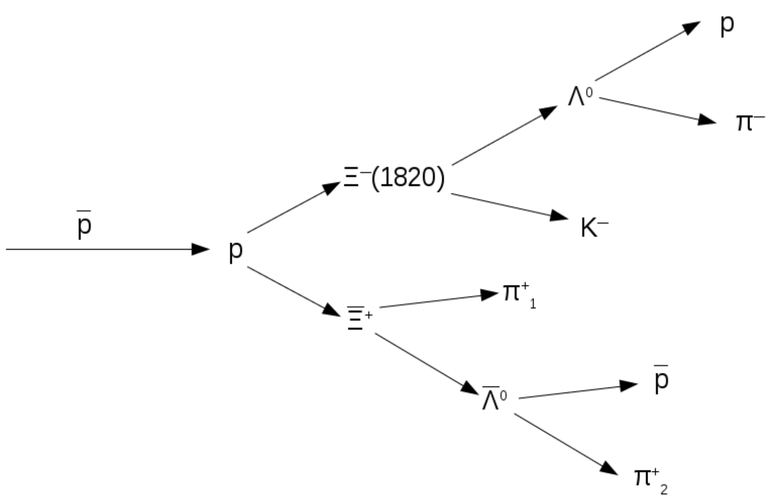

Figure 1.1: Simulated decay channel

For the charge conjungated channel were also 1.5 million signal events generated. The parameter which are used for the event generation are shown in table 1.1.

The chosen beam momentum value is 100 MeV over the production threshold of $\Xi\,(1820)$ and $\bar{\Xi}$. The production cross section is expected to be of the same order ($\sim \mu\,\mathrm{b}$) as for Ξ [1].

Table 1.1: Parameter for event generation

Parameter	Value
Beam momentum	4.6 GeV/c^2
Production	PHSP
Tracking	Ideal
Particle ID	Ideal

The used software versions for Pandaroot and the external software is listed in table 1.2

Table 1.2: Used software versions

Software	Version
FairSoft	mar15
FairRoot	v-15.03a
PandaRoot	trunk revision 28555
Geant	3
Genfit	1

The $\Xi\,(1820)$ was not defined in the evt.pdl file. The Lines in the code sniplet 1.1 shown how the particle was added to the file. As the properties of $\Xi\,(1820)$ I am using the values which are shown in table 1.3. These values are taken from [2].

Listing 1.1: sniplet from evt.pdl

```
add  p Particle Xi(1820)- 23314 1.8230000e+00 2.4000000e-02
   2.0000000e-01 -3 3 0.0000000e+00 23314
add  p Particle anti-Xi(1820)+ -23314 1.8230000e+00 2.4000000e-02
    2.0000000e-01 3 3 0.0000000e+00 -23314
```

The generated transverse momentum against the longitudinal momentum for Λ^0, $\bar{\Lambda}^0$, $\bar{\Xi}$ and $\Xi\,(1820)$ is presented in figure 1.2
Figure 1.4 shows the Dalitz plot for the Λ^0, K^- and $\bar{\Xi}$ final states for the channel $\bar{\mathrm{p}}\mathrm{p} \rightarrow \Xi\,(1820)\ \bar{\Xi}$.

Table 1.3: Values for $\Xi\,(1820)$ and $\bar{\Xi}\,(1820)$ from [2]

Particle	J	I	P	Charge	Mass	Width
$\Xi\,(1820)$	$\frac{3}{2}$	$\frac{1}{2}$	(-1)	(-1)	$(1.823 \pm 5)\mathrm{GeV/c^2}$	(0.024 ± 6) GeV
$\bar{\Xi}\,(1820)$	$\frac{3}{2}$	$\frac{1}{2}$	(-1)	1	$(1.823 \pm 5)\mathrm{GeV/c^2}$	(0.024 ± 6) GeV

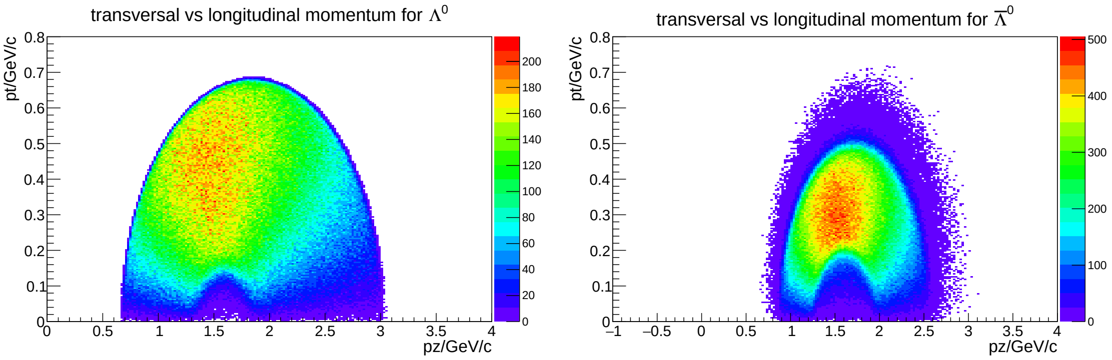

(a) Λ^0 (b) $\bar{\Lambda}^0$

Figure 1.2: Figure a) shows transversal against the longitudinal momentum distribution for Λ^0. Figure b) transversal versus longitudinal momentum distribution for $\bar{\Lambda}^0$.

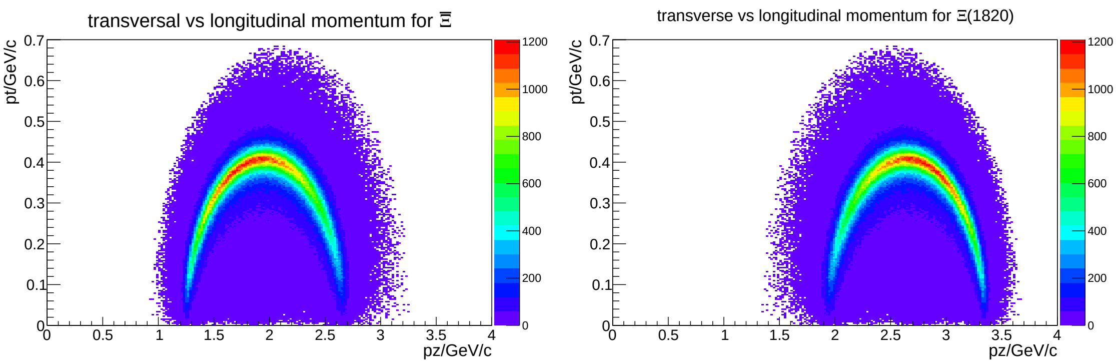

(a) $\bar{\Xi}$ (b) $\Xi\,(1820)$

Figure 1.3: Figure a) shows transversal against the longitudinal momentum distribution for $\bar{\Xi}$. Figure b) transversal versus longitudinal momentum distribution for $\Xi\,(1820)$.

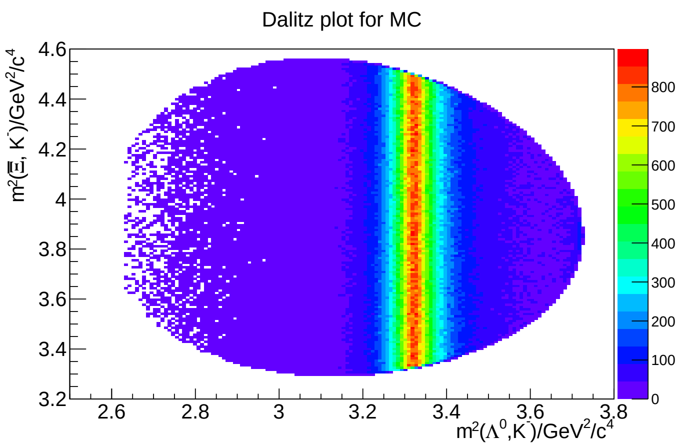

Figure 1.4: Dalitz plot for simulation. On x axis is the mass square of Λ^0 and K^- and on the y axis there is the mass square of $\bar{\Xi}$ and K^-

2 Analysis

To reconstruct all the simulated particles we start with the final state particles and go backwards through the reaction chain.

2.1 Final state particle

The selected final state particle are protons, antiproton, π^-, π^+, K^- and K^+ mesons. For the reconstruction of these final state particles I used an ideal tracking. To make the selection a bit more realistic only particles with more than 3 hits in any inner tracking detector (MVD, STT and GEM) are selected. The selection criterion is chosen because three hits are defining a cirlce. A fourth hit point is than a validation of the track hypothesis.
The particle identification (PID) is also ideal. The selection criterion is set to 'best'.
The reconstruction efficieny for the final state particle is shown in table 2.1 and figure

2.1.
Table 2.2 shows the reconstruction efficiency for the c.c. channel.

2.2 Reconstruction of Λ^0 and $\bar{\Lambda}^0$

Selection

For the reconstruction of

- Λ^0 a proton and a π^- meson are combined and

Table 2.1: reco efficiency and momentum resolution for $\bar{\mathrm{p}}\mathrm{p} \to \Xi\,(1820)\,\bar{\Xi}$

final state	N/%	$\frac{\sigma p}{p}$/%
π^-	83.48	1.53
π_1^+ ($\bar{\Xi}$)	80.93	1.38
π_2^+ ($\bar{\Lambda}^0$)	83.07	1.49
K^-	78.59	1.58
p	84.39	1.61
$\bar{\mathrm{p}}$	78.25	1.61

Table 2.2: reco efficiency and momentum resolution for $\bar{\mathrm{p}}\mathrm{p} \rightarrow \bar{\Xi}\,(1820)\ \Xi$

final state	N/%	$\frac{\sigma p}{p}$/%
π^{+}		
π_1^{-} (Ξ)		
π_2^{-} (Λ^0)		
K^{+}		
p		
$\bar{\mathrm{p}}$		

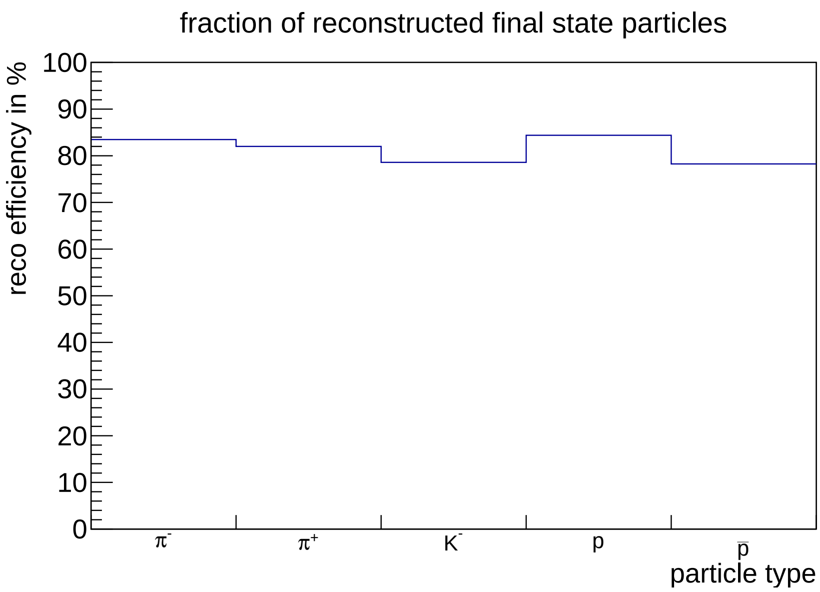

Figure 2.1: Reconstruction efficiency for final state particles. The x axis shows the particle type. On the y axis is shown the fraction of reconstructed particles, like it is shown in table 2.1

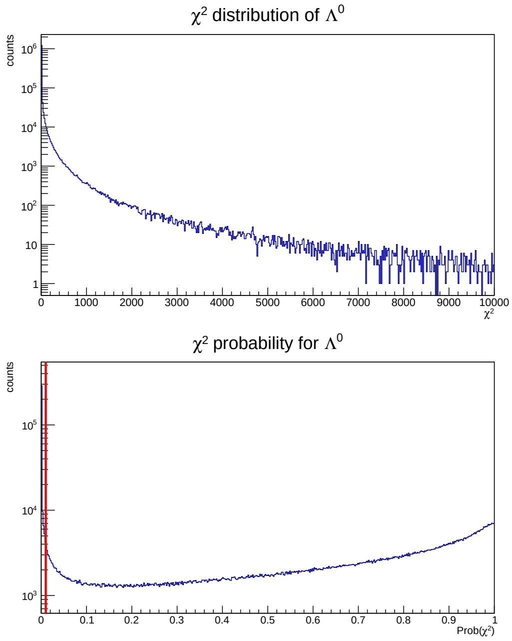

Figure 2.2: upper: χ^2 distribution; lower: χ^2 probability distribution

- for the reconstruction of $\bar{\Lambda}^0$ a $\bar{\text{p}}$ and a π^+ are combined.

After the combination of the daughter particles a mass window cut is performed. Only those particles are chosen which have a mass within 0.3GeV/c^2.
A vertex constraint fit with the PndKinVertexFitter is performed on the selected particle. This means that the tracks of the daughter particles are fitted to a common vertex point. The χ^2 and χ^2-Probability distiribution of the vertex fit for Λ^0 is shown in figure 2.2.
In the χ^2-probability distribution one can see a increasing number of events for probabilites going to one. These feature is not coming from vertex fitting. There is still a problem with covariance matrices which causes the effect.

The fit information coming from the vertex fit are used to perform a mass contraint fit with the kinematic fitter PndKinFitter. After using both fitter the selection criterion is set. One select only those particles which have a probabiltiy greater than 1% in both fitter. A scheme which shows how the events are selected can be found in figure 2.3.
If there is more than one candidate left after the cuts the best fitted candidate is chosen.

Results

This subsection presents the results for the Λ^0 and $\bar{\Lambda}^0$ selection with the selection criteria introduced above. The mass distributions for different cuts are shown in figure 2.4 and figure 2.5.

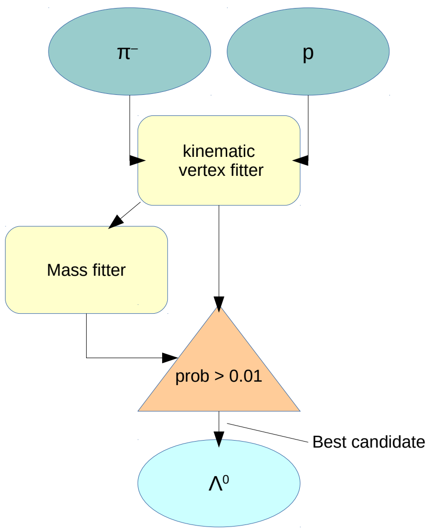

Figure 2.3: Scheme for Λ^0 reconstruction

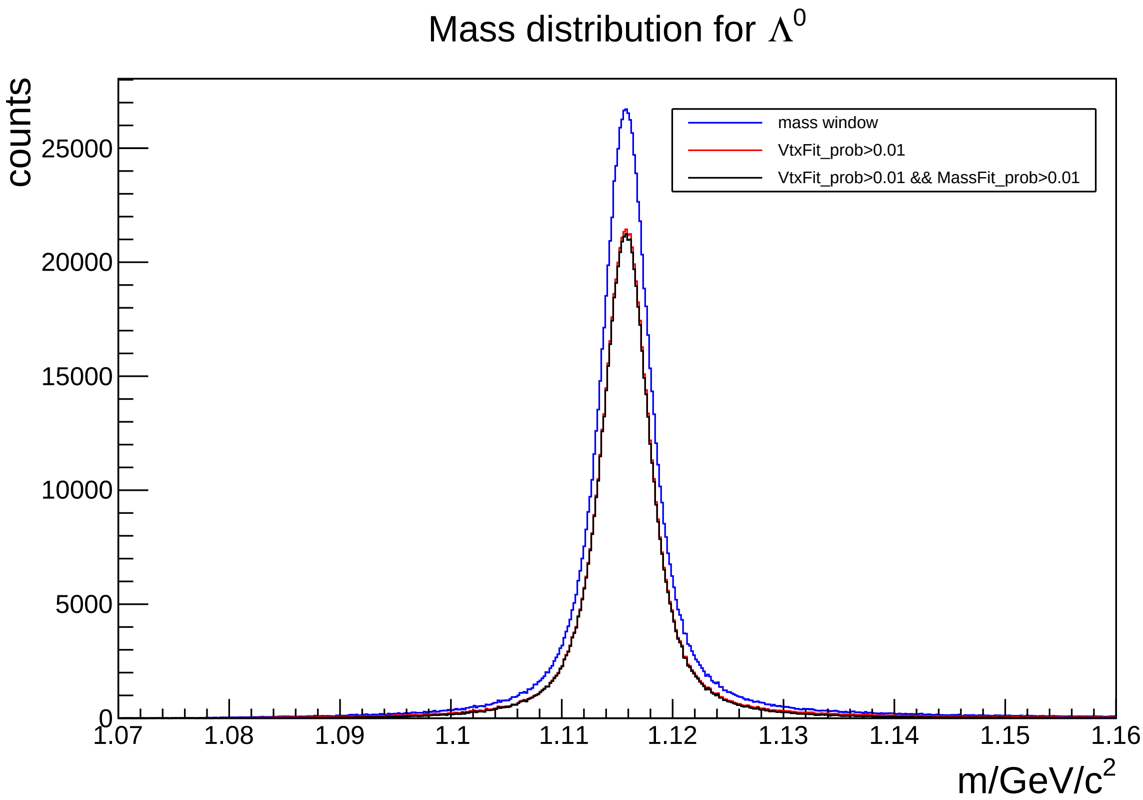

Figure 2.4: Mass distribution of Λ^0 for different cuts

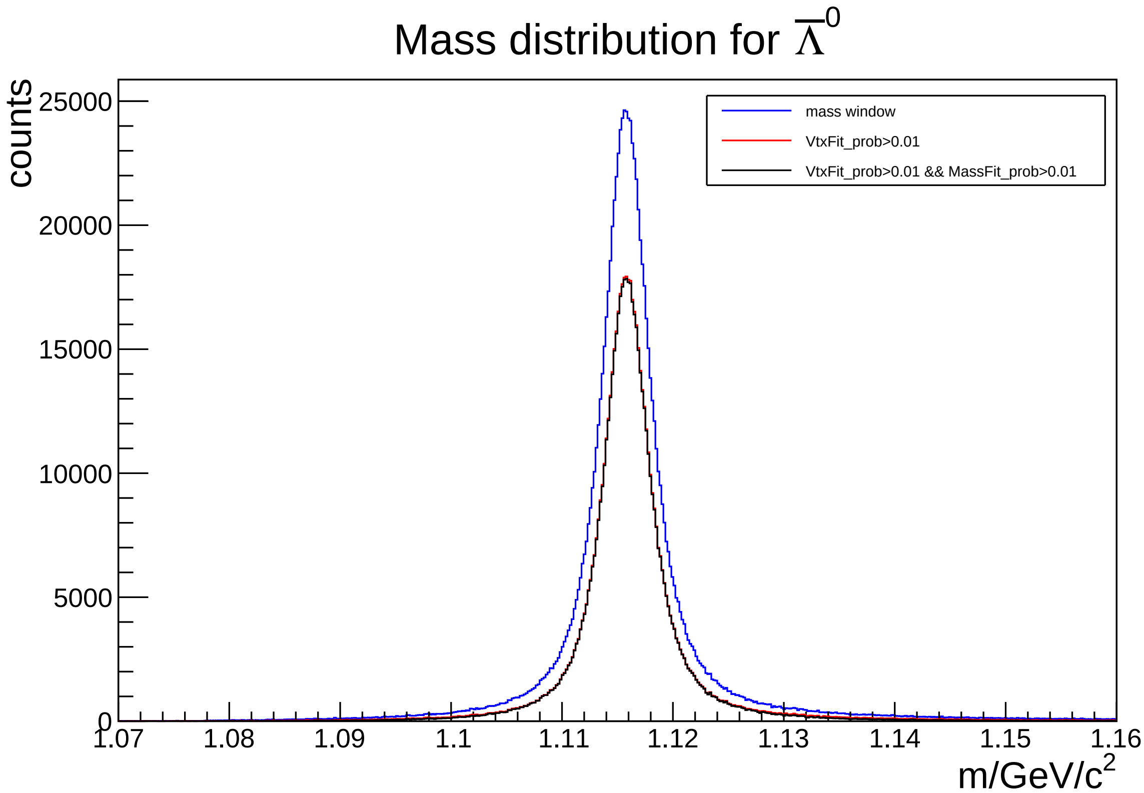

Figure 2.5: Mass distribution of $\bar{\Lambda}^0$ for different cuts

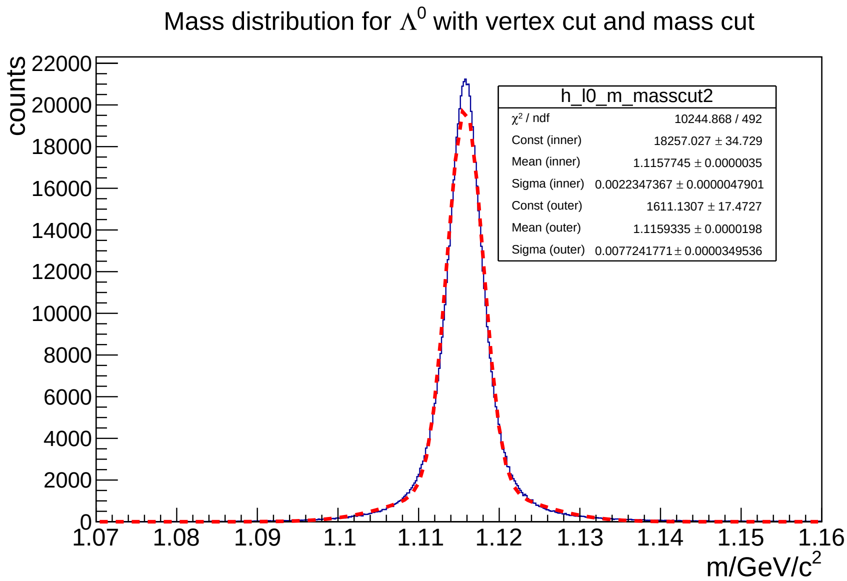

Figure 2.6: Mass distribution – blue line – for Λ^0 fitted with a double gaussian fit shown as red dashed line.

The reconstructed mass can be derived by performing a doulbe gaussian fit on the cutted mass. The mass distribution and the double gausssian fit are exemplarily shown for Λ^0 in figure 2.6

The mean value of the inner gaussian fit is the reconstructed mass. The result for Λ^0 is $m_{\Lambda^0} = \left(1.116 \pm 3.5 \cdot 10^{-5}\right)$ GeV/c^2 and for $\bar{\Lambda}^0$: $m_{\bar{\Lambda}^0} = \left(1.116 \pm 1 \cdot 10^{-5}\right)$GeV/c^2. The small fit errors could be a result from the wrong covariance matrices. But this has to be checked. Figure 2.7 shows the transverse momentum versus the longitudinal momentum. After all cuts the reconstruction efficiency for Λ^0 is 50.33% and for $\bar{\Lambda}^0$ 41.46%. The

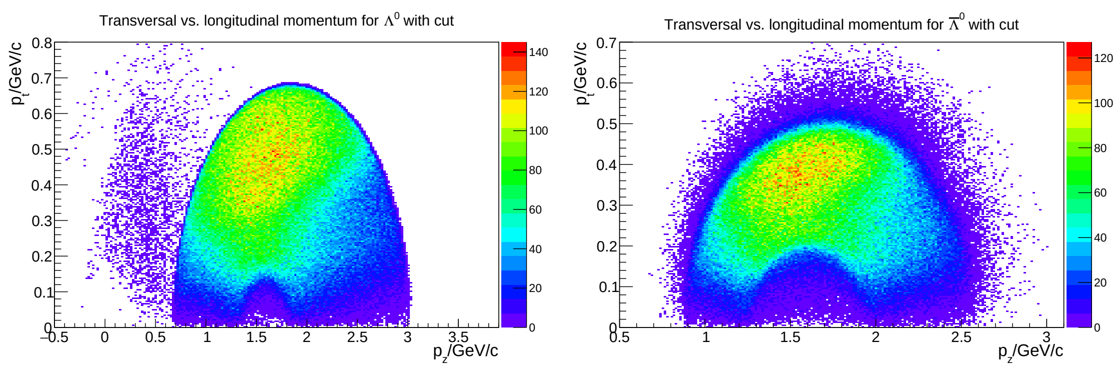

(a) (b)

Figure 2.7: The plots shows the transverse against the longuitudinal momentum for Λ^0

Table 2.3: Vertex resolution for $\bar{\Xi}$ and Ξ (c.c. channel)

position	$\bar{\Xi}$	cascade(from c.c.)
x	0.03282 ± 0.00017	
y	0.03326 ± 0.00017	
z	0.12054 ± 0.00058	

difference of the reconstruction efficiency of Λ^0 and $\bar{\Lambda}^0$ is caused by the difference between the decay length of their mother particles. Λ^0 is emitted by the $\Xi\,(1820)$ which has a very short decay length while the decay length of Ξ and $\bar{\Xi}$ is $c\tau = 4.91\,\text{cm}$ [2]. In addition the decay length of Λ^0 and $\bar{\Lambda}^0$ is $c\tau = 7.98\,\text{cm}$. If one sum this number up the final state particles of $\bar{\Lambda}^0$ are produced more downstream than the final state particles of Λ^0. This can be also seen in figure 2.8. The finale state particles coming from $\bar{\Lambda}^0$ are produced at the edge of the MVD detector so that the reconsturction efficiency get worse.

2.3 Reconstruction of Ξ and $\bar{\Xi}$

Selection

The reconstruction of Ξ and $\bar{\Xi}$ fellow a simila scheme like for Λ^0 and $\bar{\Lambda}^0$. For $\bar{\Xi}$ are $\bar{\Lambda}^0$ and π_1^+ recombined and for Ξ in the c.c. channel Λ^0 and π_1^-. Now it is distinguished between the to π^+ (π^-) particle and use only those particles which have not already been combined. After combining the daughter particles it is performed a mass window cut with width of 0.3GeV/c^2 arraound the Ξ mass $m_\Xi = 1.32171$ GeV/c^2 [2].
The fitting scheme is the same as for Λ^0 and $\bar{\Lambda}^0$ and is shown in figure 2.9 After the mass window cut the daughter particles are fitted to a common vertex with the PndKinVtxFitter. And again these information are given into the mass constraint fitter.
Only these particles are selected which have a probability of more than 1 % in both fitter. Figure 2.10 shows exemplarily the cut on the vertex fit probability.
If there is more than one candidate left after all cuts the best candidate is chosen.

Results

The vertex resolution after all cuts is shown in table table 2.3.
It is determined by performing a Gaussian fit to the peak of the distribution. The sigma of the fit gives the vertex resolution. Figure 2.11 and Figure 2.12 show the vertex resolution with the Gaussian fit.
The mass distribution for the different cuts is shown in figure 2.13 and figure 2.14. The vertex fitter cut reduces the number of events most and the width of the mass distribution

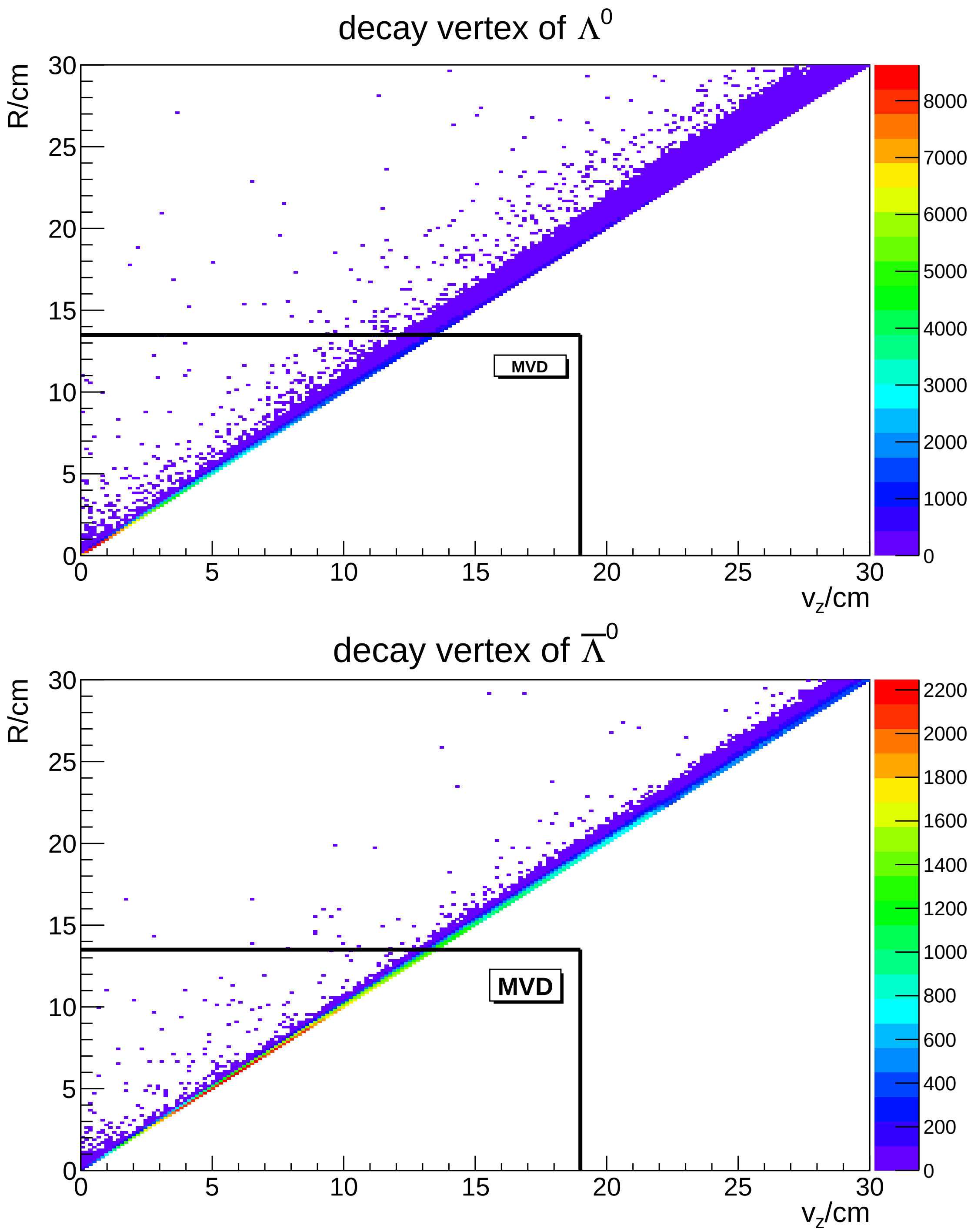

Figure 2.8: Upper plot shows the decay vertex of Λ^0; lower plot shows decay vertex of $\bar{\Lambda}^0$

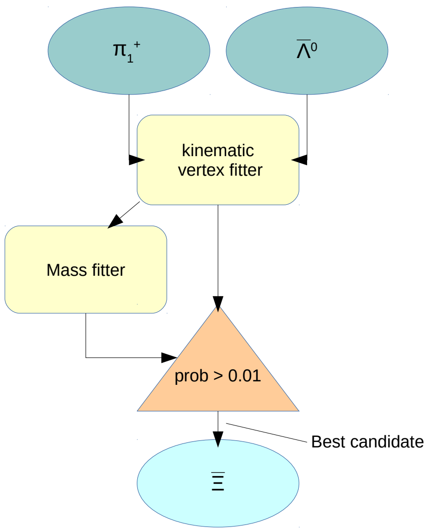

Figure 2.9: Scheme for $\bar{\Xi}$ reconstruction

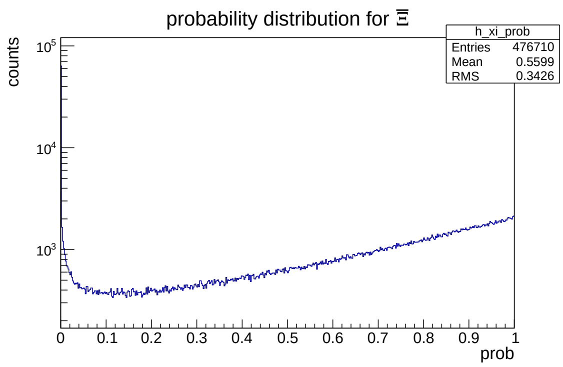

Figure 2.10: χ^2 probalility for $\bar{\Xi}$ reconstruction

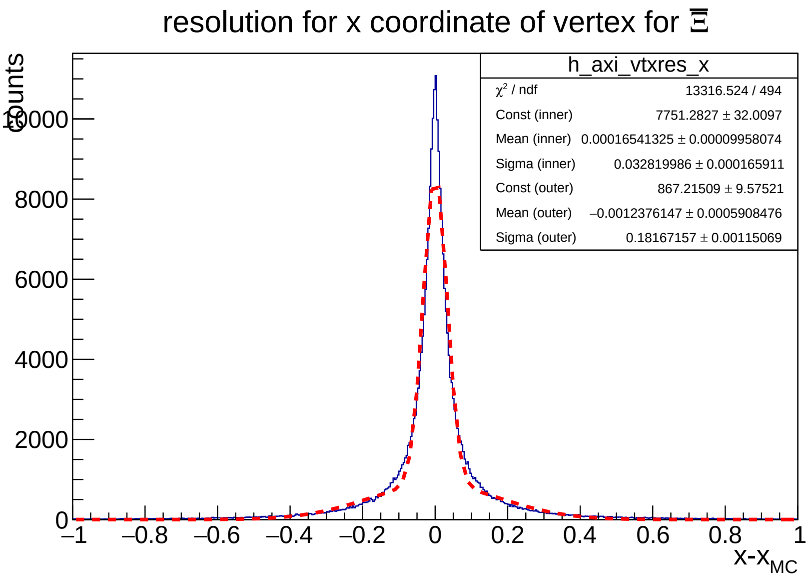

Figure 2.11: Vertex resolution of x position for $\bar{\Xi}$

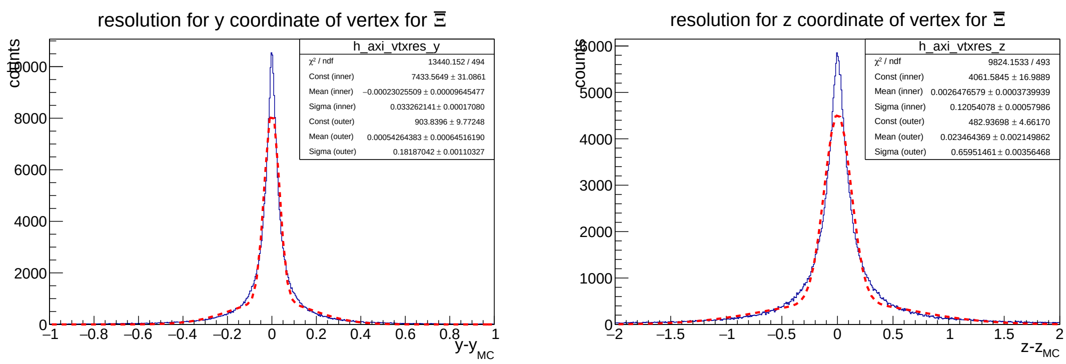

(a) (b)

Figure 2.12: left plot: Vertex resolution of y position for $\bar{\Xi}$; right plot: Vertex resolution of z position for $\bar{\Xi}$.

gets smaller.
After using all cuts on the mass distribution the reconstructed mass of Ξ and $\bar{\Xi}$ can be determined by a double Gaussian fit. This is exemplarily shown in figure 2.15.
The result of the mass fit is for $\bar{\Xi}$ m $= \left(1.3721716 \pm 9.2 \cdot 10^{-5}\right)$ GeV/c^2 and for Ξ m $= \left(1 \pm 1 \cdot 10^{-5}\right)$ GeV/c^2. The two dimensional momentum distribution for $\bar{\Xi}$ and Ξ is shown in figure 2.16
The reconstruction efficiency for $\bar{\Xi}$ is 18.39% and for Ξ 18.64%.

2.4 Reconstruction of Ξ(1820) and $\bar{\Xi}$(1820)

Combination

-daughter particles for Ξ (1820): Λ^0 and K^- meson
-daughter particles for $\bar{\Xi}$ (1820): $\bar{\Lambda}^0$ and K^+
-using best candidate from Λ^0 and $\bar{\Lambda}^0$
-K^+ and K^- with more than 3 Hits in one subdetector
-performing a mass window cut with width of 0.3GeV/c^2

Fitting

- fitting particles to common vertex with PndKinVtxFitter
- only select particles with prob bigger than 0.01
- scheme in figure 2.17
-if there is more than one particle, choose best candidate
- χ^2 probability distribution for vertex fit shown in figure 2.18

Results

- mass for different cuts see figure 2.19
- mass fit figure 2.20

2.5 Reconstruction of hole chain

combination

-using best candidate from Ξ (1820) and $\bar{\Xi}$
-for c.c : $\bar{\Xi}$ (1820) and Ξ
-mass window of 0.3GeV/c^2

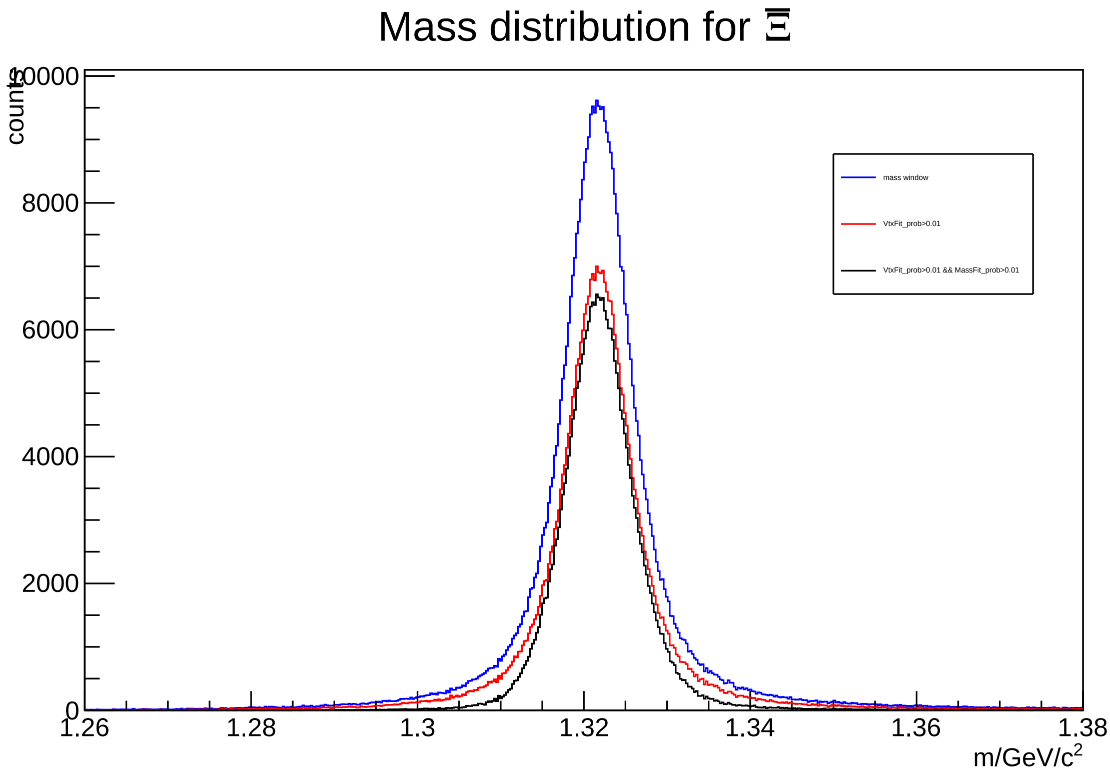

Figure 2.13: Mass distribution of $\bar{\Xi}$ for different cuts

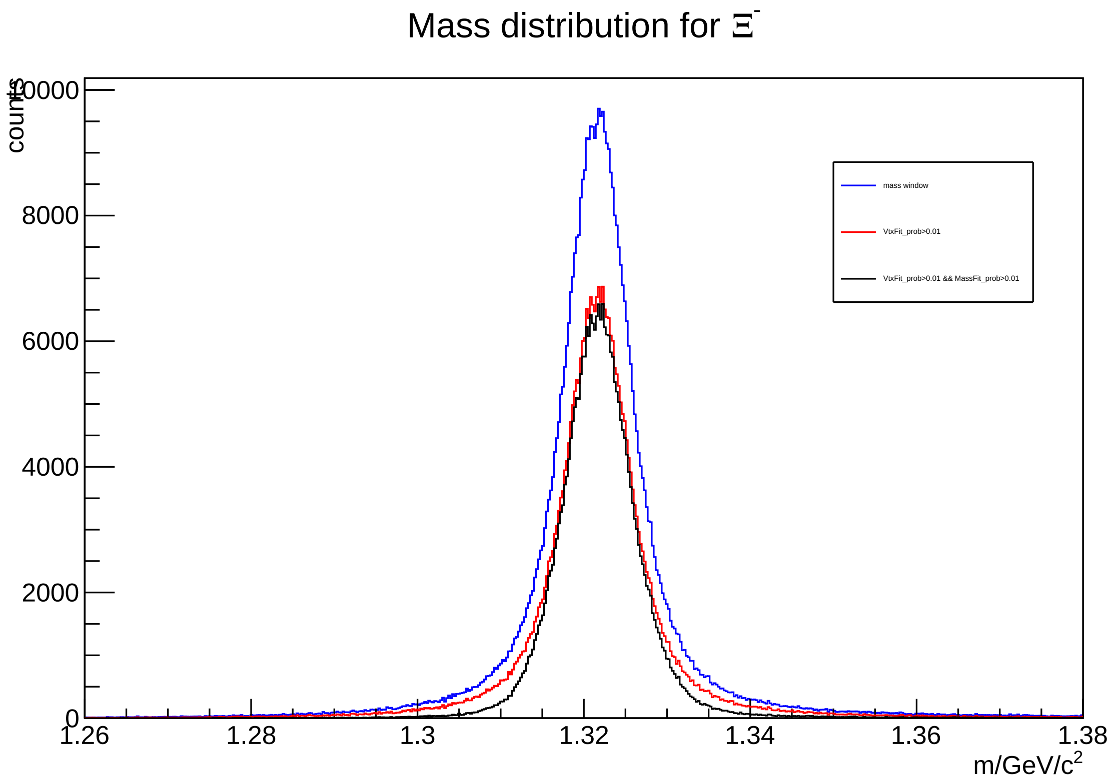

Figure 2.14: Mass distribution of Ξ for different cuts

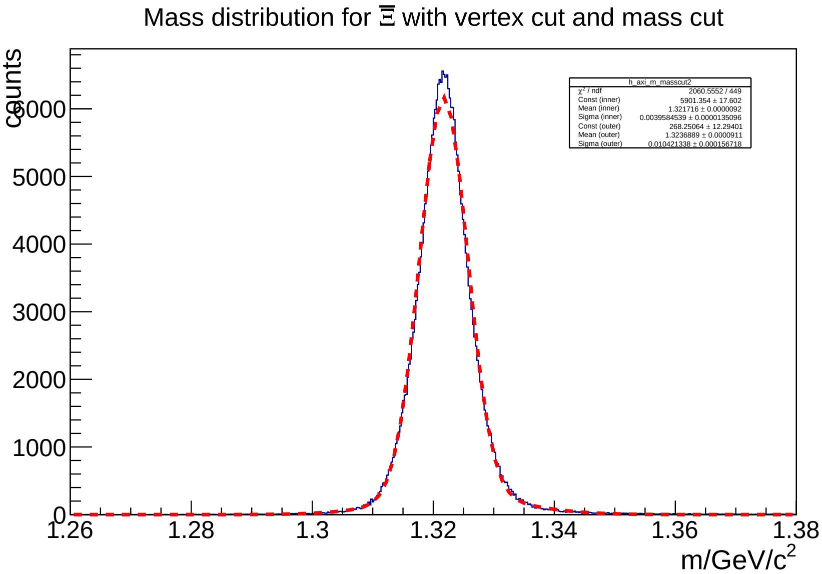

Figure 2.15: Mass fit with a double gaussian fit

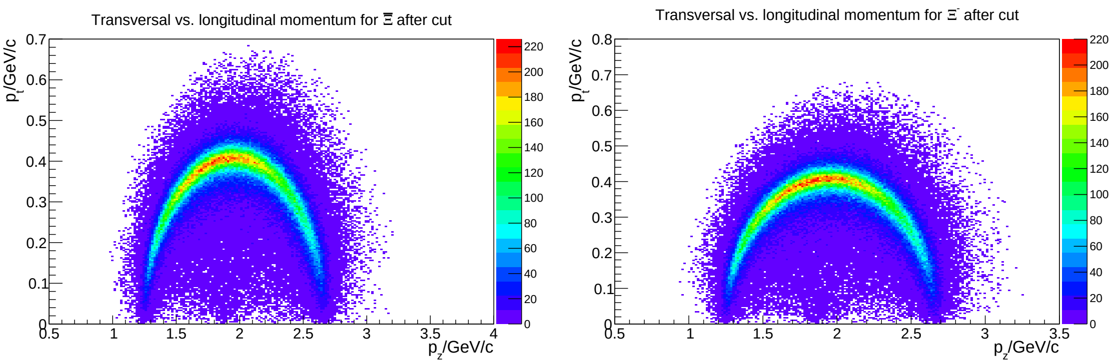

(a) $\bar{\Xi}$

(b) Ξ

Figure 2.16: The plots shows the transverse against the longuitudinal momentum for $\bar{\Xi}$ and Ξ

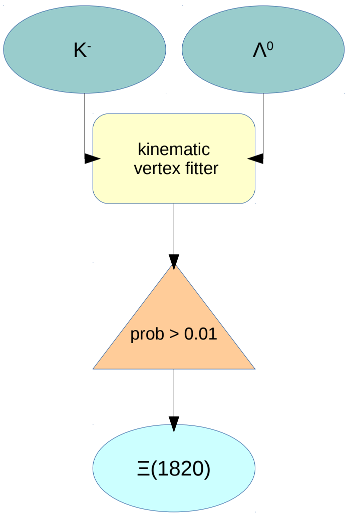

Figure 2.17: Scheme for $\Xi\,(1820)$ reconstruction

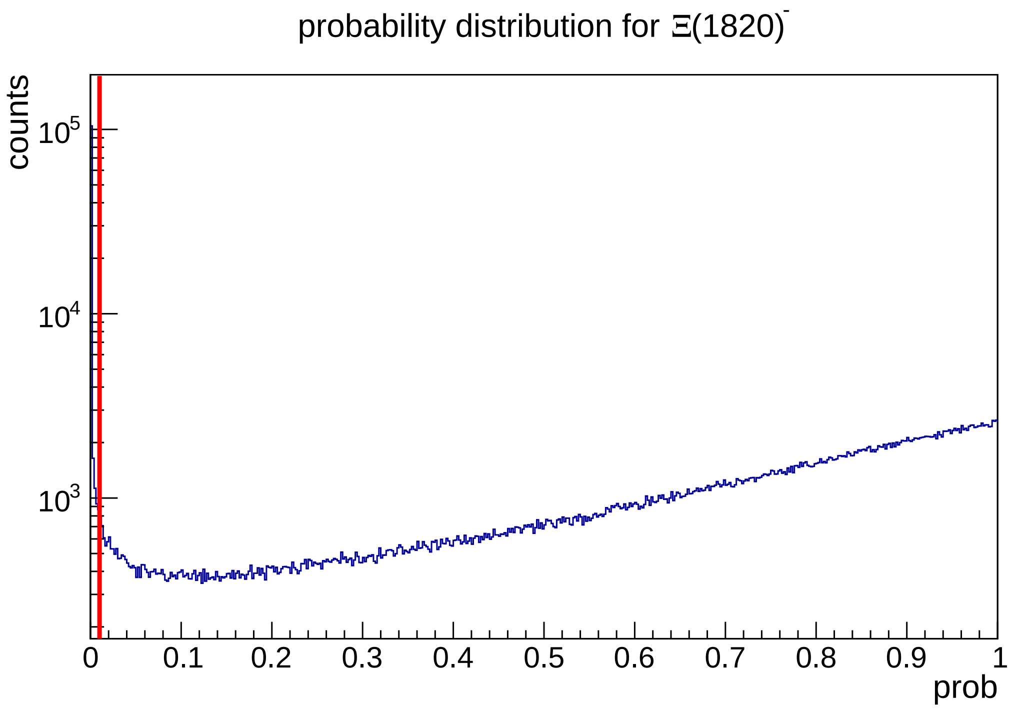

Figure 2.18: χ^2 probability distribution of kinematic vertex fit for $\Xi\,(1820)$.

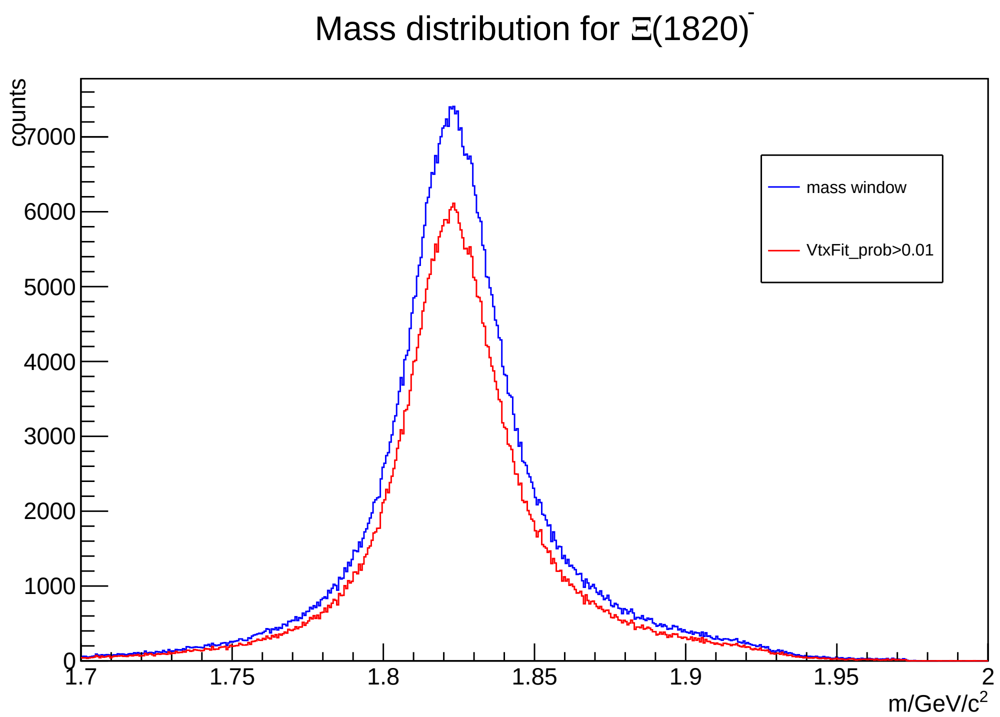

Figure 2.19: Mass distribution for $\Xi\,(1820)$ for the different cuts

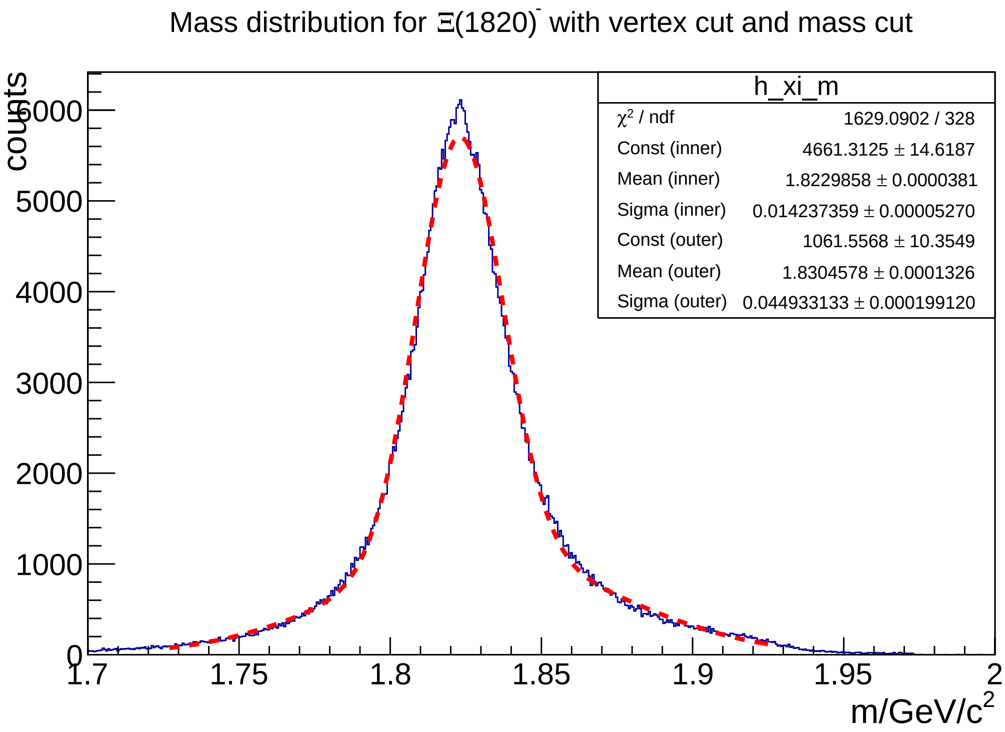

Figure 2.20: Mass distribution after all cuts for Ξ (1820).

Figure 2.21: 4-constraint fit probability

Fitting

-use PndKinFitter with four momentum constrained
-initial four momentum vector is

$$(p_x, p_y, p_z, E) = (0, 0, 4.6, 5.63)$$

-if probability is better than 1% keep candidate
-scheme shown in figure 2.22
- table 2.4 shows summary of reconstruction efficiency for non-final state particles
- dalitz plot is shown in figure 2.23

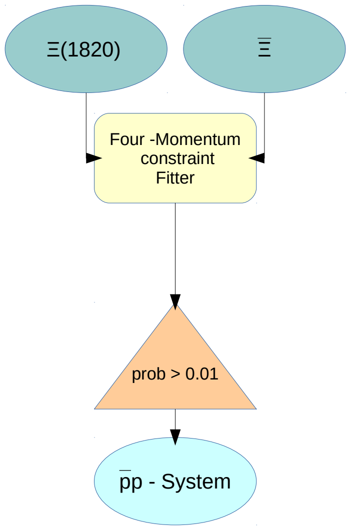

Figure 2.22: Scheme for 4-Constraint Fit

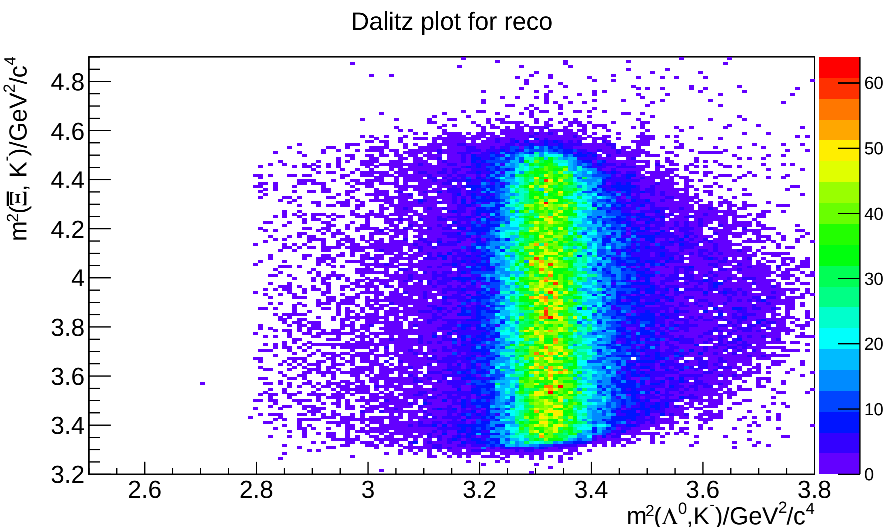

Figure 2.23: Dalitz plot for reconstructed particles

Table 2.4: reconstruction efficiency for non-final state particles for $\bar{p}p \rightarrow \Xi\,(1820)\;\bar{\Xi}$

particle	reco efficiency in %	dp/p in %
Λ^0		
$\bar{\Lambda}^0$		
$\bar{\Xi}$		
$\Xi\,(1820)$		
$\bar{\Xi}\;\Xi$ system		

3 Background

Bibliography

[1] W. Erni, I. Keshelashvili, B. Krusche, M. Steinacher, Y. Heng, Z. Liu, H. Liu, X. Shen, O. Wang, H. Xu, *et al.*, “Physics performance report for panda: Strong interaction studies with antiprotons,” *arXiv preprint arXiv:0903.3905*, 2009.

[2] J. B. et al., *Particle Data Group.* Phys. Rev. D86, 010001, 2012.